Mn and V co-doped Li₂FeSiO₄ Cathode Materials with Enhanced Electrochemical Properties

Maolin Zhang*, *Huicong Hu, Jing Li, Dongyan Zhang, Yangxi Yan, Zhimin Li*

School of Advanced Materials and Nanotechnology, Xidian University, Xi'an, 710071, China
*E-mail: mlzhang@xidian.edu.cn

Co-substitution at Fe site has been shown to enhance electrochemical properties of Li₂FeSiO₄-based cathode materials. Hence, Mn and V co-doped $Li_2Fe_{0.8(1-x)}Mn_{0.2(1-x)}V_xSiO_4$ (x=0, 1%, 2%, and 5%) were prepared in this study through citrate-assisted sol-gel method. Effects of Mn and V co-substitution on structures, morphologies, and electrochemical behaviors of obtained materials were investigated by X-ray diffraction (XRD), scanning electron microscopy (SEM), charge-discharge testing, and AC impedance measurements. The results indicated that specimens with doping content of x=1% displayed the best initial discharge specific capacity of 134.5 mAh/g at 0.1 C rate with retention capacity over 80% after 100 cycles. These improvements were linked to several factors, including lamellar-like particle morphology, electrochemical activity of V-ion, high Li-ion diffusion coefficient, and large exchange current.

1. INTRODUCTION

Lithium-ion batteries (LIBs) are widely used in 3C products like computers, communication, and consumer electronics, as well as in power sources of electric vehicles and energy storage devices for renewable energy and smart grids [1-2]. Cathode materials are key components of LIBs, affecting their electrochemical performances. Layered $LiCoO_2$ [3], spinel $LiMn_2O_4$ [4] and olivine $LiFePO_4$ [5] have widely been employed in various areas due to their high reversibility features, elevated energy densities, and long cycle life. Besides, Li₂FeSiO₄ are good candidates for next-generation power sources thanks to their superior thermal stabilities attributed to strong Si-O bonding and elevated theoretical specific capacities issued from one or two Li^+ extractions with 166/332 mAh/g, respectively [6-10].

Li₂FeSiO₄ has been first synthesized and characterized as cathode material for LIBs by Nyten [11]. The excellent performances of Li₂FeSiO₄ encouraged its further improvement worldwide. However, its poor electronic conductivity (10^{-13} S/cm) and low Li-ion diffusion coefficient (10^{-17} cm²/s)

limited its widespread application [12-14]. Moreover, the real discharge specific capacity of Li_2FeSiO_4 still much lower than the theoretical value. Therefore, tremendous efforts have been devoted to further enhance the electrochemical properties of Li_2FeSiO_4 based cathode materials.

Doping is an effective way to improve the electrochemical properties of Li_2FeSiO_4. Numerous studies have reported that the introduction of foreign atoms into unit cells should produce lattice defects, further improving the electronic conductivity and ion-diffusion coefficient. Li_2FeSiO_4 can undergo more than one Li-ion de-intercalation when transition metal M is oxidized from M^{2+} to M^{4+}/M^{5+} through replacement of Fe element, leading to increased discharge capacities [15]. Various doping ions, such as Mg^{2+} [16], Ni^{2+} [17], Y^{3+} [18], Mn^{2+} [19] and V^{3+} [20] have successfully been tested. The big similarity in radius and electronegativity of Fe^{2+} (76 pm and 1.83 eV) and Mn^{2+} (80 pm and 1.55 eV) renders insertion of Mn in Fe lattice of Li_2FeSiO_4 structure possible. Furthermore, Mn doping could enhance the structural stability and decrease potential polarization, leading to increased initial discharge specific capacity [21-22]. Therefore, Mn^{2+} doping attracted increasing attention in Li_2FeSiO_4 cathode materials for LIBs [23]. However, the optimum doping concentration is not entirely uniform due to variation in synthesis route, processing, and starting reactants. On the other hand, the Jahn-Teller effect of Mn^{3+} induces serious fading in crystal stability and obvious decay in cycling performance [20, 22, 24-27]. $Li_2Fe_{0.5}Mn_{0.5}SiO_4$ showed initial discharge capacity of 214 mAh/g but with capacity lost over 40% after 10 cycles [28].

On the other hand, doping with high valence state cation ions could enhance the electrical and ionic conductivities, leading to improved diffusion properties of Li ions and increased rate performance of batteries [29]. Substitution of vanadium (V) improves the extraction capacity of Li ion to yield smaller band gaps, hence improving electron conductivity [14, 20]. Doping with V also enhances the specific capacity thanks to formation of several oxide states as high as +5 [14-15]. Using first-principle calculations, Liivat has recorded that intercalation voltages of $Li_2FeSi_{0.875}V_{0.125}O_4$ was less than 3.2 V with extra specific capacity around 12.5% [30]. Cheng found $Li_xFe_{0.5}V_{0.5}SiO_4$ to display minimum capacity fading due to small strain in cell parameters of the crystal [15].

To further enhance the electrochemical properties of Li_2FeSiO_4, co-doping with different cations has been confirmed to be effective. Toyama recorded $Li_{2.2}Fe_{0.4}Mn_{0.4}Si_{0.8}V_{0.2}O_4$ with initial discharge capacity of 197 mAh/g while $Li_2Fe_{0.5}Mn_{0.5}SiO_4$ delivered only 134 mAh/g [31]. However, they did not test for other electrochemical performances, such as rate and cycling properties. Gao prepared Mn and Al co-doped Li_2FeSiO_4 by solid-state method with improved capacity retention despite slight decrease in discharge capacity [32]. Similar results were observed with Mn and Mg/Zn co-doped Li_2FeSiO_4 cathode materials [33].

In this work, Mn and V co-doped $Li_2Fe_{0.8(1-x)}Mn_{0.2(1-x)}V_xSiO_4$ (x=0, 1%, 2% and 5%) cathode materials were prepared by citrate-assisted sol-gel method. The phase structures, morphologies and electrochemical characteristics were all studied and the results were discussed. The optimum doping ratios were determined based on the electrochemical properties.

2. EXPERIMENTAL

2.1 Preparation

Citrate-assisted sol-gel method was used for synthesis of Mn and V co-doped $Li_2Fe_{0.8(1-x)}Mn_{0.2(1-x)}V_xSiO_4$ (x=0, 1%, 2% and 5%) to yield cathode materials. All reagents were of analytical grade and purchased from China National Pharmaceutical Group Co., Ltd. $LiNO_3$, $Fe(NO_3)_3$, $Mn(NO_3)_2$, and $C_6H_8O_7$ were used as starting reactants, which were dissolved in deionized water to obtain precursor solution. V_2O_5 was dissolved in diluted ammonia as chelating agent and doping ion, which then was added into the precursor solution under strong magnetic stirring. The pH value of mixed solution was adjusted to 3 by adding ammonia. TEOS was used as silica source and added to the mixed solution at 80 °C under stirring for 24 h until formation of wet gel followed by oven drying at 100 °C. The dried powder was next calcined at 650 °C for 10 h under nitrogen atmosphere to yield Mn and V co-doped Li_2FeSiO_4 cathode materials.

The prepared cathode materials were mixed with conductive agent (acetylene black) and binder (PVDF) at weight ratio of 80:10:10, and then pasted on aluminum foil to yield the positive electrodes of LIBs. Li metal was used as anode, microporous polypropylene membrane (Celgard 2400) as separator, and $LiPF_6$ as electrolyte. Coin cells (CR-2016) were fabricated to test the electrochemical performances of prepared cathode materials. The fabrication process of CR-2016 cells was achieved according to the literatures [34-36].

2.2 Characterization

The phase structures of obtained powders were characterized by X-ray diffraction (XRD, D8 Advance, Bruker, Germany) over 2θ range of 10-75° and step of 0.02°. The morphologies were observed by scanning electron microscopy (SEM, JSM-7500F, Jeol, Japan). The charge and discharge tests of coin cells were recorded by multichannel galvanostatic system (CT2001A, Lanhe, China) between 1.5 and 4.3 V at various scanning rates. Electrochemical impedance spectroscopy (EIS) measurements were conducted by CHI660E electrochemistry workstation (Chinstruments, China) at voltage amplitude of 5 mV and frequency range of 10^{-2} - 10^5 Hz.

3. RESULTS AND DISCUSSION

Figure 1 shows the XRD patterns of prepared cathode samples. At low V-doping content (less than 5%), the powders obviously showed monoclinic structure with Pmn21 space group. In addition, no impurity phases were recorded, indicating incorporation of Mn and V atoms into Li_2FeSiO_4 crystal lattice. However, some impurity peaks appeared when doping content increased to 5%, and crystal orientation of materials changed. On the other hand, the characteristic diffraction peak of pure Li_2FeSiO_4 at 24.32 ° slightly shifted to higher angles, suggesting slight reduction in lattice parameters according to Bragg equation since ion radius of V^{3+} (74 pm) was smaller than those of Mn^{2+} (80 pm) and Fe^{2+} (76

pm). Indeed, the change was very weak and inadequate due to small amounts of V dopant content. These results agreed well with those reported by Dominko [20], Deng [26], and Guo [22]. Nevertheless, Cheng [15] and Liivat [30] confirmed that V substitution would improve the electronic conductivity of Li_2FeSiO_4 due to decreased bandgap (Eg).
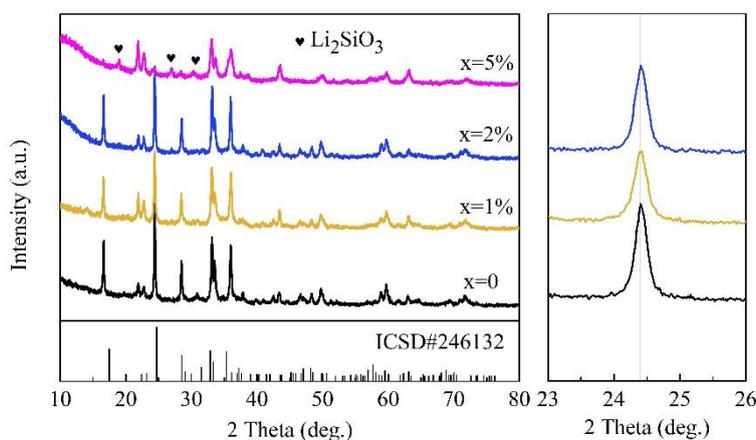
Figure 1. XRD patterns of prepared $Li_2Fe_{0.8(1-x)}Mn_{0.2(1-x)}V_xSiO_4$ (x=0, 1%, 2% and 5%) cathode powders.

The morphologies of as-prepared powders are depicted in Figure 2. The morphologies obviously underwent drastic change as doping amount varied. Using single doping of Mn (x=0), the morphology of prepared powder looked spherical with particle size around 100 nm. The introduction of V in $Li_2Fe_{0.8}Mn_{0.2}SiO_4$ induced lamellar-like particles, which vanished as V content increased. The reason for this had to do with introduction of impurity phase at high V-doping contents (5%). In general, lamellar-like particles helped to reduce the diffusion distance of Li ions and enhance the electrochemical performances.
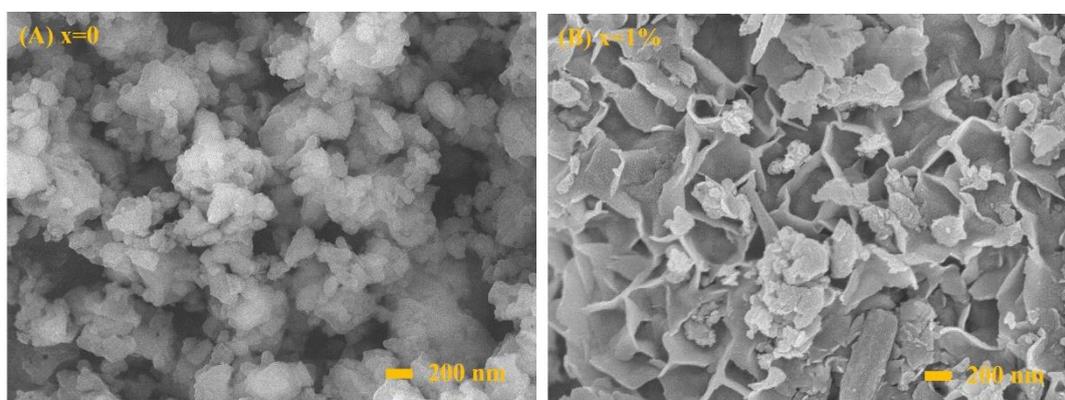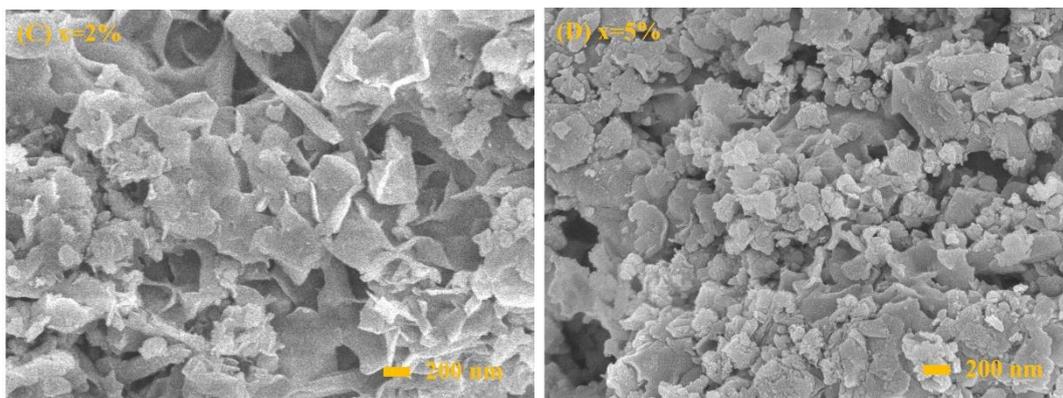
Figure 2. SEM images of $Li_2Fe_{0.8(1-x)}Mn_{0.2(1-x)}V_xSiO_4$ (x=0, 1%, 2% and 5%) cathode materials.

EIS was used to better clarify the electrochemical properties of co-doped powders. As shown in Figure 3 (A), all curves consisted of typically depressed semicircles in high-frequency region and lines in low-frequency region. The intercept at Z′-axis at high frequencies corresponds to ohmic resistance (R_s) and semicircle in middle-frequencies is attributed to charge transfer resistance (R_{ct}) linked to charge transfer at electrode/electrolyte interface [37-38]. The line in low-frequency region is related to Li-ion diffusion. The results of EIS fitted by Z-View software are presented in Table 1. R_s value looked almost the same as dopant content changed. However, R_{ct} values were very different and recorded as 301.2, 98.5, 200.4, and 652.5 Ω for $Li_2Fe_{0.8(1-x)}Mn_{0.2(1-x)}V_xSiO_4$ (x=0, 1%, 2% and 5%) specimens, respectively. Hence, addition of suitable V-ion content would decrease charge-transfer resistance, further enhancing the electrochemical properties. Moreover, the exchange current density was calculated by Eq. (1) [39-40]:

$$ i = \frac{RT}{nFR_{ct}} \qquad (1) $$

where R, T, n and F represent the gas constant, absolute temperature, number of electrons per reaction species and Faraday constant, respectively. As shown in Table 1, $Li_2Fe_{0.8(1-x)}Mn_{0.2(1-x)}V_xSiO_4$ (x=1%) displayed the highest exchange current density. Therefore, charge-transfer reaction can be enhanced by incorporating appropriate Mn and V to yield better electrochemical performances.

To further clarify the kinetic of Li^+ intercalation and de-intercalation of co-doped cathode materials during charge and discharge processes, the diffusion coefficients of Li^+ (D_{Li}) were calculated from the relationship between impedance real part (Z′) and $\omega^{-1/2}$ at low frequencies. D_{Li} can be calculated by Eq. (2) [38, 40-41]:

$$ D_{Li} = \frac{R^2T^2}{2A^2n^4F^4C^2\sigma^2} \qquad (2) $$

where A and C represent the electrode surface area and molar concentration of Li ions. σ is Warburg coefficient obtained from the line relationship of Z′ and $\omega^{-1/2}$ (Figure 3(B)) [16, 39, 42]. The diffusion coefficients were calculated as 8.3×10^{-14}, 1.2×10^{-13}, 1.3×10^{-13} and 3.2×10^{-14} cm^2/s for samples $Li_2Fe_{0.8(1-x)}Mn_{0.2(1-x)}V_xSiO_4$ (x=0, 1%, 2% and 5%), respectively. These results agreed well with previous work reported by Gao [40], and could be attributed to suitable co-doping of V/Mn and lamellar-like particle

of active powders. In sum, V and Mn co-doping showed positive effect on electrochemical performances of cathode materials.
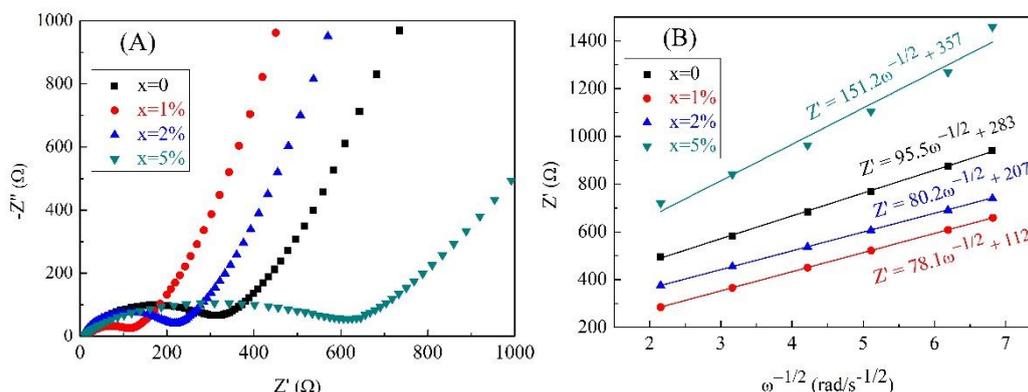
Figure 3. (A) Nyquist plot of $Li_2Fe_{0.8(1-x)}Mn_{0.2(1-x)}V_xSiO_4$ (x=0, 1%, 2% and 5%) and (B) relationship between Z' and $\omega^{-1/2}$ in low-frequency range.

Table 1. Parameters of $Li_2Fe_{0.8(1-x)}Mn_{0.2(1-x)}V_xSiO_4$ (x=0, 1%, 2% and 5%) specimens obtained from EIS.

Samples	R_s (Ω)	R_{ct} (Ω)	i (A)	D_{Li} (cm^2/s)
x=0	13.9	301.2	0.86×10^{-4}	8.3×10^{-14}
x=1%	17.5	98.5	2.62×10^{-4}	1.2×10^{-13}
x=2%	16.9	200.4	1.29×10^{-4}	1.3×10^{-13}
x=5%	17.2	652.5	0.40×10^{-4}	3.2×10^{-14}
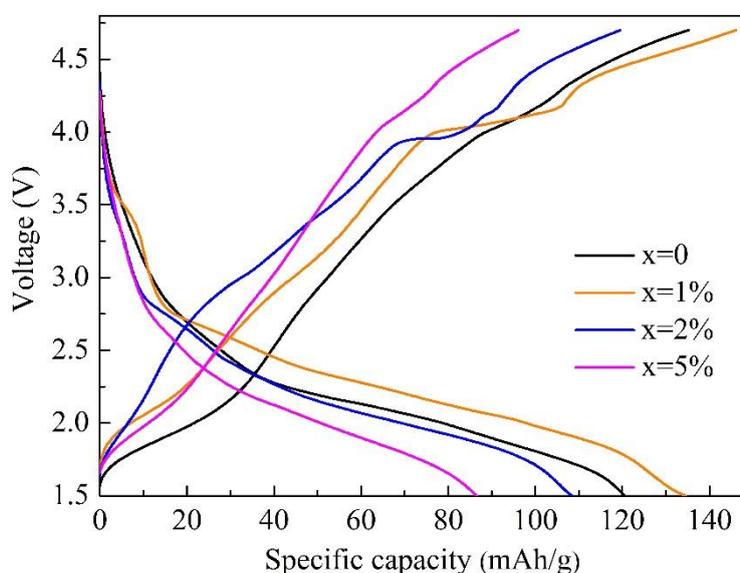
Figure 4. Initial charge-discharge properties of $Li_2Fe_{0.8(1-x)}Mn_{0.2(1-x)}V_xSiO_4$ (x=0, 1%, 2% and 5%) cathode materials at 0.1 C rate.

Figure 4 displays the initial charge-discharge performances of prepared cathode materials at room temperature. As V doping rose, the initial discharge specific capacity first increased and then decreased. The initial charge/discharge specific capacities of $Li_2Fe_{0.8(1-x)}Mn_{0.2(1-x)}V_xSiO_4$ (x=0, 1%, 2% and 5%) were recorded as 135.2/120.5 mAh/g, 146.1/134.5 mAh/g, 119.5/108.4 mAh/g and 92.1/86.6 mAh/g, respectively. It has been reported that Mn^{2+}/Mn^{3+} and Mn^{3+}/Mn^{4+} redox couples occurred at high voltage oxidation peak of 4.4 and 4.8 V, respectively [43]. In subsequent cycles, the peaks moved obviously to lower voltages [33]. Accordingly, the enhanced initial specific capacity might originate from redox reactions due to V doping.

For pure Li_2FeSiO_4, only one potential plateau was observed at 2.8 V and associated with Fe^{2+}/Fe^{3+} oxidation reaction. Cheng reported four peaks at 2.30, 2.87, 3.14 and 3.35 V, corresponding to V^{2+}/V^{3+}, Fe^{2+}/Fe^{3+}, V^{3+}/V^{4+} and V^{4+}/V^{5+} redox couples [15], respectively. Therefore, Mn and V co-doped electrode materials exhibited slope voltage profiles over the entire range, corresponding to multiple electrochemical reactions. In addition, the coulombic efficiencies defined as ratio of discharge/charge capacity during cycling of $Li_2Fe_{0.8(1-x)}Mn_{0.2(1-x)}V_xSiO_4$ (x=0, 1%, 2% and 5%) were estimated to 89.1%, 92.1%, 90.7% and 94.3%, respectively. The highest initial coulombic efficiency was obtained for sample x=5% due to its lowest charge and discharge capacity.

Rate performances of $Li_2Fe_{0.8(1-x)}Mn_{0.2(1-x)}V_xSiO_4$ (x=0, 1%, 2% and 5%) active materials were measured and the results are displayed in Figure 5. At each rate, charge and discharge processes were cycled for five times between 1.5-4.3 V. Sample x=1% exhibited the highest discharge capacities at various rates with specific discharge capacities of 134.5, 114.7, 98.9, and 81.5 mAh/g at 0.1 C, 0.2C, 0.5C and 1C, respectively (Figure 4(A)). It also delivered the highest discharge capacity of 33.7 mA h/g at 4 C rate, much larger than those of sample x=0 (21.3 mA h/g), x=2% (20.0 mA h/g) and x=5% (14.2 mA h/g). This good rate capability was attributed to lowest kinetic barrier associated with highest diffusion coefficient of Li^+. In general, migration time of Li-ion (t_{Li}) is strongly related to diffusion length (L) and diffusion coefficient (D_{Li}) of active materials, as shown in Eq. (3) [44-45]:

$$t_{Li} = \frac{L^2}{D_{Li^+}} \qquad\qquad (3)$$

Active materials with smaller particle size would often have shorter Li-ion diffusion pathway. Therefore, sample x=0 showed better rate capability than sample x=2% despite its elevated diffusion coefficient. On the other hand, presence of some impurities led to unstable crystal structure during charge/discharge processes, yielding worst rate performance.

The discharge potential profiles at different rates showed active materials with considerably lower working voltages at increasing C rates (Figure 5(B-D)), suggesting significant increase in electrode resistance and serious energy fade upon discharging at higher current densities. Hence, not suitable for practical applications in EVs and power tools due to low Li-ion diffusion ability of olivine-type crystal structure of Li_2FeSiO_4. Nevertheless, the active material $Li_2Fe_{0.8(1-x)}Mn_{0.2(1-x)}V_xSiO_4$ (x=1%) displayed limited fading at each discharge rate, demonstrating lower electrode resistance and faster Li-ion diffusion speed material.
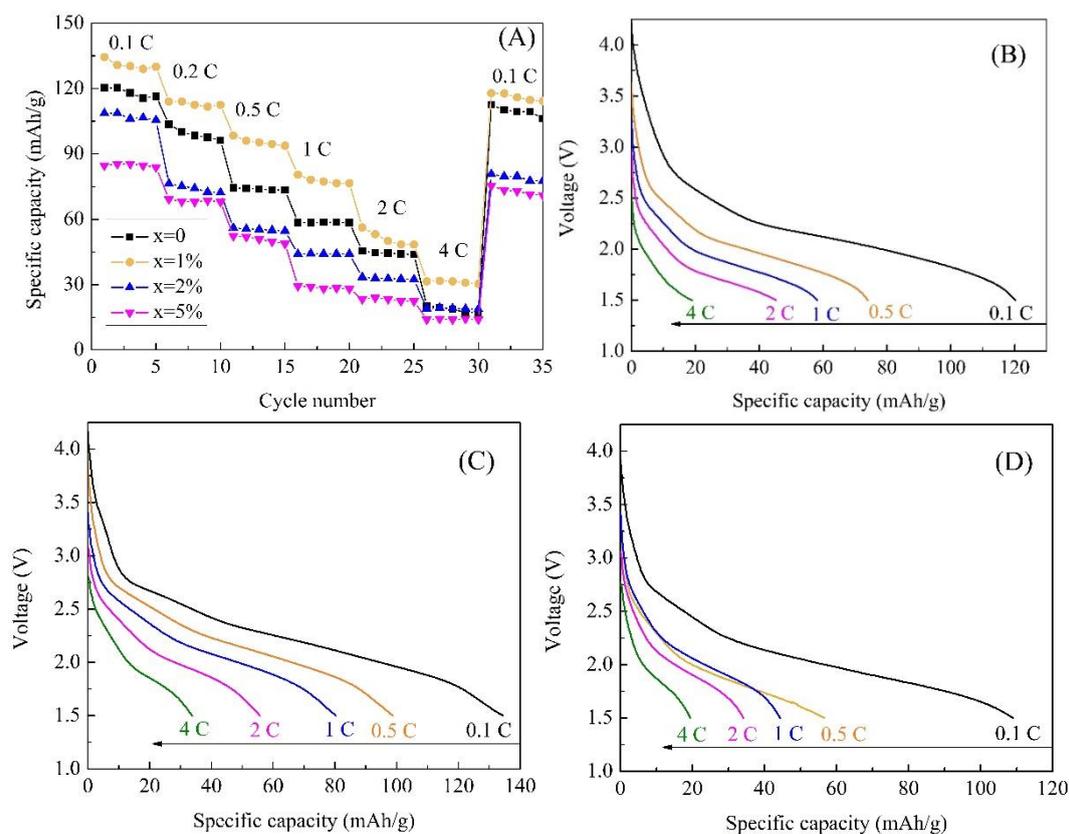
Figure 5. Rate performances (A) and discharge behaviors (B-D) of various $Li_2Fe_{0.8(1-x)}Mn_{0.2(1-x)}V_xSiO_4$ (x=0, 1% and 2%) cathode materials.

Figure 6 (A) shows the cycle performances of co-doped $Li_2Fe_{0.8(1-x)}Mn_{0.2(1-x)}Si_{1-x}V_xO_4$ (x=0, 1%, 2%, 5%) after 100 cycles at 0.1 C rate. The doping content was strongly associated with cycle life characteristics. Sample $Li_2Fe_{0.8(1-x)}Mn_{0.2(1-x)}V_xSiO_4$ (x=1%) displayed an initial charge specific capacity of 134.5 mAh/g with 107.2 mAh/g remained after 100 cycles at room temperature (capacity retention 80%). However, the initial discharge capacities of other samples were not only lower but the capacity retentions of both $Li_2Fe_{0.8}Mn_{0.2}SiO_4$ and $Li_2Fe_{0.8(1-x)}Mn_{0.2(1-x)}V_xSiO_4$ (x=2%) decreased to 76% and 78%, respectively. Thus, Mn and V co-doping can effectively improve the cycle performance when compared to single Mn-doped specimen. However, the capacity retention decreased to 70% when V-doping content increased to 5% due to formation of impurity phase in crystal structure. Nevertheless, the coulombic efficiencies of all prepared active materials remained fairly constant at 100% after several cycles. Moreover, the potential profile of sample $Li_2Fe_{0.8(1-x)}Mn_{0.2(1-x)}V_xSiO_4$ (x=1%) decreased very slowly, indicating that suitable co-doping would inhibit voltage drop during Li^+ intercalation and de-intercalation processes.

As shown in Table 2, Mn and Mg co-doped $Li_2Fe_{0.75}Mn_{0.2}Mg_{0.05}SiO_4$ has previously showed discharge capacities reaching of 118 mAh/g with corresponding capacity retention of 63.5%. Similarly, capacity retention of $Li_2Fe_{0.7}Mn_{0.2}Z_{0.1}SiO_4$ reached 69.5% in spite of lower discharge capacity of 55.3 mAh/g after 50 cycles [33]. Mn and Al co-doped $Li_2Fe_{0.75}Mn_{0.2}Al_{0.05}SiO_4$ showed an initial discharge capacity of 159.3 mAh/g with capacity retention of 78% after 50 cycles [32]. The redox reaction of V-ion in crystal lattice rendered the dopant electrochemically active. Therefore, discharge properties of Mn

and V co-doped active powders greatly improved. However, the initial specific capacity requires further enhancement if compared to values reported by Toyama due to low V-doping content [31].

Table 2. Electrochemical properties of typical co-doped Li_2FeSiO_4 based cathode materials.

Samples	First cycle discharge capacity	Coulombic efficiency	Capacity retention rate	Reference
$Li_2Fe_{0.792}Mn_{0.198}V_{0.01}SiO_4$	134.5 mAh/g at 1/10 C	92.1%	80% after 100 cycles	This work
$Li_{2.2}Fe_{0.4}Mn_{0.4}Si_{0.8}V_{0.2}O_4$	197 mAh/g at 1/20 C	95.1%	No report	31
$Li_2Fe_{0.75}Mn_{0.2}Mg_{0.05}SiO_4$	118 mAh/g at 1/16 C	86%	63% after 50 cycles	32
$Li_2Fe_{0.7}Mn_{0.2}Z_{0.1}SiO_4$	96.8 mAh/g at 1/ 16 C	88%	69% after 50 cycles	32
$Li_2Fe_{0.75}Mn_{0.2}Al_{0.05}SiO_4$	159.3 mAh/g at 1/16 C	89%	78% after 50 cycles	33
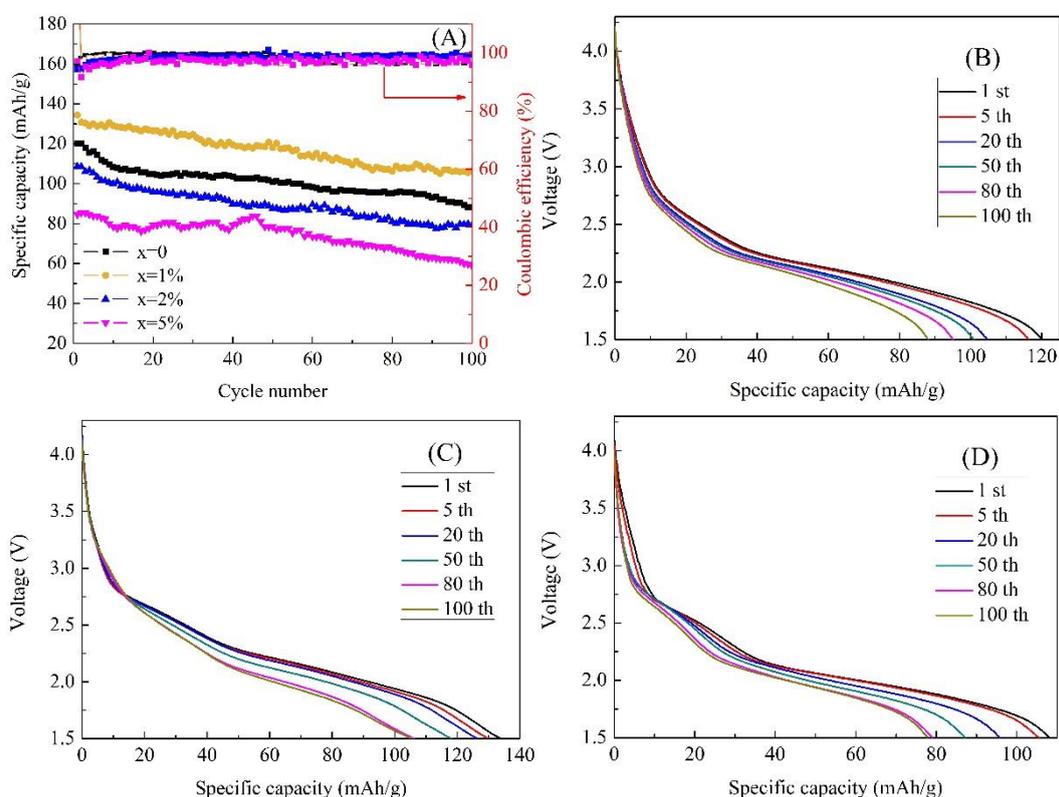
Figure 6. Cycling performance (A) and discharge properties after different cycles (B-D) of as-prepared $Li_2Fe_{0.8(1-x)}Mn_{0.2(1-x)}V_xSiO_4$ (x=0, 1%, 2% and 5%) cathode materials fabricated with Li metal as anode.

4. CONCLUSIONS

To improve the electrochemical properties by synergistic effect, Mn and V co-doped $Li_2Fe_{0.8(1-x)}Mn_{0.2(1-x)}V_xSiO_4$ (x=0, 1%, 2%, and 5%) cathode materials were prepared by citrate-assisted sol-gel

method. The co-doped samples were all indexed to space group Pmn21 with similar lattice parameters at varied dopant contents. Lamellar-like particles were obtained by introducing suitable dopant content (x=1%). V-doping improved Li-ion diffusion coefficient and exchange current due to enhanced electrochemical activity during intercalation and de-intercalation processes of Li-ion. Specimen with doping content of x=1% displayed best initial discharge specific capacity reaching 134.5 mAh/g at 0.1 C rate with capacity retention of 80% after 100th cycling.

References

1. M. Gaikwad, B.V. Khau, G. Davies, B. Hertzberg, D.A. Steingart and A.C. Arias, *Adv. Eng. Mater.*, 5 (2015) 1401389.
2. M.S. Whittingham, *Chem. Rev.*, 114 (2014) 11414.
3. C.Z. Lu, J.M. Chen, Y.D. Cho, W.H. Hsu, P. Muralidharan and T.K. Fey, *J. Power Sources*, 184 (2008) 392.
4. P. Ghosh, S. Mahanty and R.N. Basu, *Mate. Chem. Phys.*, 110 (2008) 406.
5. D. Shanmukaraj, G.X. Wang, R. Murugan and H.K. Liu, *Mater. Sci. Eng.*, 149 (2008) 93.
6. P. Larsson, R. Ahuja, A. Nytén and J.O. Thomas, *Electrochem. Commun.*, 8 (2006) 797.
7. F. Zhou, M. Cococcioni, K. Kang and G. Ceder, *Electrochem. Commun.*, 6 (2004) 1144.
8. M.S. Islam, R. Dominko, C. Masquelier and C. Sirisopanaporn, *J. Med. Chem.*, 21 (2011) 9811.
9. M. Bini, S. Ferrari, C. Ferrara, M.C. Mozzati, D. Capsoni and A.J. Pell, *Sci. Rep.*, 3 (2013) 3452.
10. C. Sirisopanaporn, C. Masquelier, P.G. Bruce and A.R. Armstrong, *J. Amer. Chem. Soc.*, 133 (2011) 1263.
11. A. Nytén, A. Abouimrane, M. Armand, T. Gustafsson and J.O. Thomas, *Electrochem. Commun.*, 7 (2005) 156.
12. R.B. Araujo, R.H. Scheicher and J.S. de Almeida, *Solid State Ionics*, 247-248 (2013) 8.
13. P. Zhang, C.H. Hu, S.Q. Wu, Z.Z. Zhu and Y. Yang, *Phys. Chem. Chem. Phys.*, 14 (2012) 7346.
14. Z. Zhang, X.Q. Liu, Y. Wu, H.Y. Zhao and B. Chen, *J. Electrochem. Soc.*, 162 (2015) 737.
15. Y.S. Li, X. Cheng and Y. Zhang, *J. Electrochem. Soc.*, 159 (2012) 69.
16. L. Qu, D. Luo, S.H. Fang, Y. Liu and L. Yang, *J. Power Source*s, 307 (2016) 69.
17. H.L. Qiu, H.J. Yue, T. Zhang, Y.M. Ju and Y.Q. Zhang, *Electrochim. Acta*, 188 (2016) 636.
18. A.Y. Shenouda and M.M.S. Sanad, *J. Electrochem. Energy*, 14 (2017) 024501.
19. M. Bini, S. Ferrari, D. Capsoni, C. Spreafico, C. Tealdi and P. Mustarelli, *J. Solid State Chem.*, 200 (2013) 70.
20. L.L. Zhang, H.B. Sun, X.L.Yang, Y.W. Wen and Y.H. Huang, *Electrochim. Acta*, 152 (2015) 496.
21. R. Dominko, C. Sirisopanaporn, C. Masquelier, D. Hanzeld and I. Arcond, *J. Electrochem. Soc.*, 157 (2010) 1309.
22. H.J. Guo, X. Cao, X.Q. Li, L.M. Li, X.H. Li and Z.X. Wang, *Electrochim. Acta*, 55 (2010) 8036.
23. L.L. Yi, X.Y. Wang, G. Wang, Y.S. Bai, M.H. Liu, X. Wang and R.Z. Yu, *Electrochim. Acta*, 222 (2016) 1354.
24. L.L. Yi, X.Y. Wang, G. Wang, Y.S. Bai and M.H. Liu, *Chem. J. Chinese U.*, 31 (2010) 2148.
25. B. Shao, Y. Abe and I. Taniguchi, *Powder technol.*, 235 (2013) 1.
26. C. Deng, S. Zhang and S.Y. Yang, *J. Alloy. Compd.*, 487 (2009) 18.
27. K. Gao, *Ionics*, 20 (2014) 809.
28. Z.L. Gong, Y.X. Li and Y. Yang, *Electrochem. Solid-State Lett.*, 9 (2006) 542.

29. H. Hao, J.B. Wang, J.L. Liu, T. Huang and A.S. Yu, *J. Power Sources*, 210 (2012) 397.
30. A. Liivat and J.O. Thomas, *Comput. Mater. Sci.*, 50 (2010) 191.
31. T. Toyama and S. Takahashi, *J. Power Sources*, 294 (2015) 312.
32. T. Li, X.T. Jiang, K. Gao, C.Y. Wang and S.D. Li, *J. Chin. Chem. Soc.*, 63 (2016) 800.
33. S.D. Li, Y. Zhao, C.Y. Wang and K. Gao, *J. Brazil. Chem. Soc.*, 27 (2016) 2011.
34. Y. Fujita, T. Hira, K. Shida, M. Tsushida, J. Liao and M. Matsuda, *Ceram. Int.*, 44 (2018) 11211.
35. Y.S. Li, J. Wang, Z.F. Zhou, Q.R. Yao, Z.M. Wang, H.Y. Zhou and J.Q. Deng, *Int. J. Electrochem. Sci.*, 14 (2019) 2822.
36. Z.Y. Li and H.L. Zhang, *Int. J. Electrochem. Sci.*, 14 (2019) 3524.
37. X.B. Huang, H.H. Chen, S.B. Zhou, Y.D. Chen, J.F. Yang, Y.R. Ren, H.Y. Wang, M.Z. Qu, Z.L. Pan and Z.L. Yu, *Electrochim. Acta*, 60 (2012) 239.
38. A. Kumar, O.D. Jayakumar, V.M. Naik, G.A. Nazri and R. Naik, *Solid State Ionics*, 294 (2016) 15.
39. J.L. Yang, X.C. Kang, L. Hu, X. Gong, D.P He, T. Peng and S.C. Mu, *J. Alloy. Compd.*, 572 (2013) 158.
40. H.L. Gao, L.Z. Wang, Y. Zhang, A.Q. Zhang and Y.H. Song, *Powder Technol.*, 253 (2014) 638.
41. J.L. Yang, X.C. Kang, D.P. He, T. Peng, L. Hu and S.C. Mu, *J. Power Sources*, 242 (2013) 171.
42. H.L. Qiu, K. Zhu, H.M. Li, T.T. Li, T. Zhang, H.J. Yue, Y.J. Wei and F. Du, *Carbon*, 87 (2015) 365.
43. F. Wang, Y.M. Wang, D.M. Sun, L. Wang, H.P. Jia and J. Yang, *Electrochim. Acta*, 119 (2014) 131.
44. J.H. Liu, H.Y. Chen, J.N. Xie, Z.Q. Sun, N.N. Wu and B.R. Wu, *J. Power Sources*, 251 (2014) 208.
45. P.G. Bruce, B. Scrosati and J.M. Tarascon, *Angew. Chem. Int. Edit.*, 47 (2008) 2930.